Cell Insight 2 (2023) 100124

Contents lists available at ScienceDirect

Cell Insight

journal homepage: www.journals.elsevier.com/cell-insight

Research Article

Cannabinoid receptor 2 signal promotes type 2 immunity in the lung

Tingting Liu [a,1,2], Jiaqi Liu [b,2], Hongjie Chen [c,2], Xin Zhou [e,f], Wei Fu [e,f], Ying Cao [a], Jing Yang [a,b,c,d,f,g,*]

[a] Center for Life Sciences, Academy for Advanced Interdisciplinary Studies, Peking University, Beijing, 100871, China
[b] State Key Laboratory of Membrane Biology, School of Life Sciences, Peking University, Beijing, 100871, China
[c] Peking University-Tsinghua University-National Institute of Biological Sciences Joint Graduate Program, Academy for Advanced Interdisciplinary Studies, Peking University, Beijing, 100871, China
[d] IDG/McGovern Institute for Brain Research, Peking University, Beijing, 100871, China
[e] Department of General Surgery, Peking University Third Hospital, Beijing, 100191, China
[f] Peking University Third Hospital Cancer Center, Beijing, 100191, China
[g] Institute of Molecular Physiology, Shenzhen Bay Laboratory, Shenzhen, 518055, China

HIGHLIGHTS

- Cannabinoid receptor 2 (CB2) is highly expressed in mouse and human lung ILC2s.
- CB2 and its downstream Gi signal promote the immune function of ILC2s.
- Genetic deletion of CB2 mitigates ILC2-mediated lung inflammation.

GRAPHICAL ABSTRACT

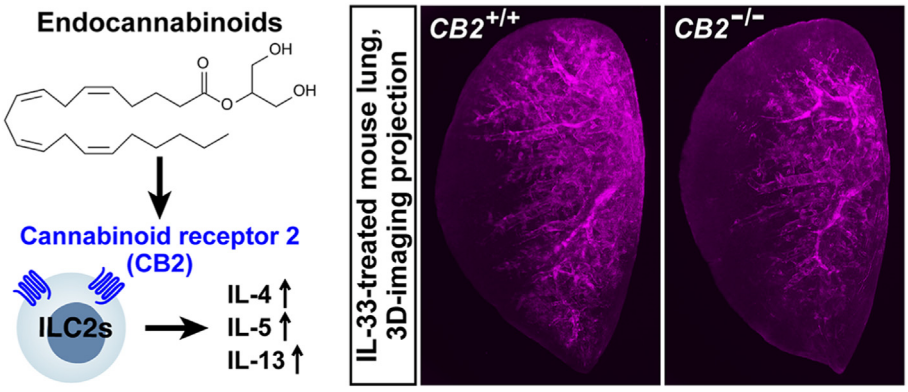

ARTICLE INFO

Keywords:
Cannabinoid receptor 2 (CB2)
Type 2 immunity
Group 2 innate lymphoid cells (ILC2s)
Lung
3D imaging

ABSTRACT

Type 2 immunity in the lung protects against pathogenic infection and facilitates tissue repair, but its dysregulation may lead to severe human diseases. Notably, cannabis usage for medical or recreational purposes has increased globally. However, the potential impact of the cannabinoid signal on lung immunity is incompletely understood. Here, we report that cannabinoid receptor 2 (CB2) is highly expressed in group 2 innate lymphoid cells (ILC2s) of mouse and human lung tissues. Of importance, the CB2 signal enhances the IL-33-elicited immune response of ILC2s. In addition, the chemogenetic manipulation of inhibitory G proteins (Gi) downstream of CB2 produces a similarly promotive effect. Conversely, the genetic deletion of CB2 mitigates the IL-33-elicited type 2 immunity in the lung. Also, such ablation of the CB2 signal ameliorates papain-induced tissue inflammation.

* Corresponding author. Center for Life Sciences, Academy for Advanced Interdisciplinary Studies, Peking University, Beijing, 100871, China.
E-mail address: jing.yang@pku.edu.cn (J. Yang).
[1] Present Address: Department of Biochemistry, Weill Cornell Medical College, New York, NY 10065, the United States.
[2] Authors contributed equally to this work.

https://doi.org/10.1016/j.cellin.2023.100124
Received 30 August 2023; Received in revised form 4 October 2023; Accepted 4 October 2023
Available online 6 October 2023

Together, these results have elucidated a critical aspect of the CB2 signal in lung immunity, implicating its potential involvement in pulmonary diseases.

1. Introduction

The lung is in direct contact with the outer environment and gets constantly challenged by a diversity of air-borne pathogens or allergens. Therefore, lung immunity must be highly effective and precisely controlled, which would otherwise cause severe human diseases (Barnes, 2008; Holt et al., 2008; Iwasaki et al., 2017; Lloyd & Marsland, 2017). It has been broadly recognized that type 2 immunity in the lung is indispensable for protecting against pathogenic infections by fungi or helminth parasites and promoting tissue repair. Also, it is critically involved in maintaining immune homeostasis and tolerance to non-pathogenic environmental stimuli. On the other hand, dysregulation of type 2 immune responses has been the hallmark of pathological conditions such as asthma (Akdis et al., 2020; Gieseck et al., 2018; Hammad & Lambrecht, 2015).

Group 2 innate lymphoid cells (ILC2s) and T helper 2 cells (T_h2) are the central components of type 2 immunity in the lung (Artis & Spits, 2015; Barlow & McKenzie, 2019; Eberl et al., 2015; Rodriguez-Rodriguez et al., 2021). In particular, upon various scenarios of lung damage, alarmins IL-25, IL-33, or thymic stromal lymphopoietin (TSLP) are up-regulated and released to trigger the innate immune response of ILC2s. ILC2s then produce effector cytokines, primarily IL-5 and IL-13, to recruit and activate eosinophils for pathogen clearance. Also, these type 2 cytokines stimulate the proliferation of goblet cells and epithelial cells to strengthen barrier integrity. Notably, accumulating evidence has suggested that in addition to immune cues, ILC2s can also respond to neural signals. For instance, our colleagues and we reported that the sympathetic neurotransmitter norepinephrine would inhibit the immune function of ILC2s (Liu et al., 2020; Moriyama et al., 2018). On the contrary, acetylcholine, another common neurotransmitter, might enhance ILC2-mediated type 2 immunity (Chu et al., 2021). Moreover, ILC2s are modulated by specific neuropeptides such as calcitonin gene-related peptide (Sui et al., 2018) or neuromedin U (Klose et al., 2017; Wallrapp et al., 2017). Despite those research advances, whether other neural-related signals influence ILC2s remains to be explored.

The endocannabinoid system has been extensively investigated in the nervous system (Lu & Mackie, 2021; Mackie, 2008; Mechoulam & Parker, 2013). Endocannabinoids, e.g., 2-arachidonoylglycerol, act via cannabinoid receptor 1 (CB1/CNR1) and cannabinoid receptor 2 (CB2/CNR2) to control brain development, synaptic plasticity, memory, and cognition. In addition, the endocannabinoid system is involved in many neurological or psychiatric disorders, such as dementia, depression, anxiety, or addiction. Accordingly, cannabinoids, either synthetic or from the natural source of cannabis, have been commonly utilized for therapeutic benefits (Di Marzo, 2008; Di Marzo et al., 2004). While CB1 is predominantly expressed in the nervous system, CB2 is broadly present in different tissues, suggesting the participation of the endocannabinoid system in non-neural functions (Lu & Mackie, 2021; Mackie, 2008). Indeed, it has long been realized that cannabinoid signals may exert diverse immunomodulatory roles (Klein et al., 2003; Tanasescu & Constantinescu, 2010). For example, a natural cannabinoid delta-9-tetrahydrocannabinol (THC) enhances the production of TNF-α and IL-1β in macrophages stimulated by lipopolysaccharides (Shivers et al., 1994). Also, THC could trigger the apoptosis of dendritic cells (Do et al., 2004). In addition, THC inhibits the development of T_h1 cells but promotes T_h2 cells during bacterial infection (Klein et al., 2000). However, the potential impact of cannabinoid signals on lung immunity is incompletely characterized.

In this study, we observed that CB2, but not CB1, is highly expressed in ILC2s of mouse and human lung tissues. Of importance, the CB2 signal could enhance the IL-33-elicited immune response of ILC2s. In addition, the chemogenetic manipulation of inhibitory G proteins (Gi) downstream of CB2 produced a similarly promotive effect. Conversely, the genetic deletion of CB2 mitigated the IL-33-elicited type 2 immunity in the lung. Also, papain-induced tissue inflammation was ameliorated by the CB2 deletion. Together, these results have demonstrated a critical aspect of the CB2 signal in modulating lung immunity in light of the global surge of cannabis usage for medical or recreational purposes (Pacula & Smart, 2017; Page et al., 2020).

2. Results

We first determined the expression profile of *CB1* and *CB2* in the ILC2s FACS-sorted from mouse lung tissues (Fig. 1A). The quantitative real-time PCR (qPCR) revealed the exclusive expression of *CB2*, but not *CB1*, in mouse lung ILC2s (Fig. 1B). In parallel, the RNA sequencing (RNA-Seq) confirmed that *CB2* was highly expressed in mouse lung ILC2s, while *CB1* mRNA levels appeared undetectable (Fig. 1C). Further, we compared *CB1* and *CB2* levels in the FACS-sorted human lung ILC2s (Fig. 1D). Similar to that observed in the mouse counterpart, human lung ILC2s predominantly expressed *CB2* (Fig. 1E), implicating its involvement in lung type 2 immunity.

We examined the CB2 signal in modulating the immune response of ILC2s. Wild-type mice were intranasally treated with the recombinant IL-33 protein, a standard model to elicit ILC2-mediated innate immunity (Kondo et al., 2008). ILC2s were FACS-sorted from the IL-33-treated lung tissues and *in vitro* stimulated with the endocannabinoid 2-arachidonoylglycerol (2-AG), the major endogenous ligand for CB2. Of importance, the 2-AG treatment effectively boosted the ILC2 expression of effector cytokines *IL-5* and *IL-13* (Fig. 1F). It has been documented that CB2 acts primarily via downstream inhibitory G proteins (Gi) (Mackie, 2008). Therefore, we bred *Vav1-Cre; Rosa26-LSL-hM4D* mice, in which the Gi-coupled chemogenetic receptor hM4D would be expressed in immune cells, including ILC2s. ILC2s were FACS-sorted from the IL-33-treated lung tissues of this mouse line and *in vitro* triggered by the chemogenetic ligand clozapine N-oxide (CNO). Such chemogenetic activation of Gi signaling was sufficient to enhance the ILC2 expression of *IL-5* and *IL-13* (Fig. 1G). In contrast, the CNO treatment showed no effect on ILC2s isolated from the IL-33-treated lung tissues of wild-type mice (data not shown), ruling out any non-specific action of this chemogenetic ligand. These results demonstrated that CB2 and its downstream Gi signal could directly promote the IL-33-elicited immune response of ILC2s.

We next generated the $CB2^{-/-}$ mouse line to investigate the function of CB2 in lung immunity. Notably, $CB2^{-/-}$ mice showed normal morphology and tissue weight of the lung compared to those of control $CB2^{+/+}$ littermates (Fig. 2A to C). Also, the CB2 deletion did not affect 2-AG levels in the lung tissues (Fig. 2D). In addition, ILC2s and other immune cell types, e.g., eosinophils, alveolar macrophages, B cells, $CD4^+$ T cells, $CD8^+$ T cells, and natural killer (NK) cells, were unaltered in the lungs of $CB2^{-/-}$ mice (Fig. 2E and F). Furthermore, the basal expression levels of type 2 cytokines *IL-4*, *IL-5*, and *IL-13* were comparable in the $CB2^{+/+}$ and $CB2^{-/-}$ lung tissues (Fig. 3D). These results suggested that the CB2 deletion would not impinge on normal development or immune homeostasis of the lung.

We observed that the intranasal IL-33 treatment did not significantly affect the *CB2* expression in mouse lung ILC2s (Fig. 3A). On the other hand, 2-AG levels increased in the IL-33-treated lung tissues (Fig. 3B), suggesting the functional involvement of the endocannabinoid signal in this context. We thus compared the IL-33-elicited immune response of $CB2^{-/-}$ and control $CB2^{+/+}$ littermates. The IL-33-treated lung tissues of $CB2^{-/-}$ and $CB2^{+/+}$ mice had similar cell numbers of ILC2s (Fig. 3C). In line with its promotive effect on ILC2s *in vitro*, the CB2 deletion mitigated

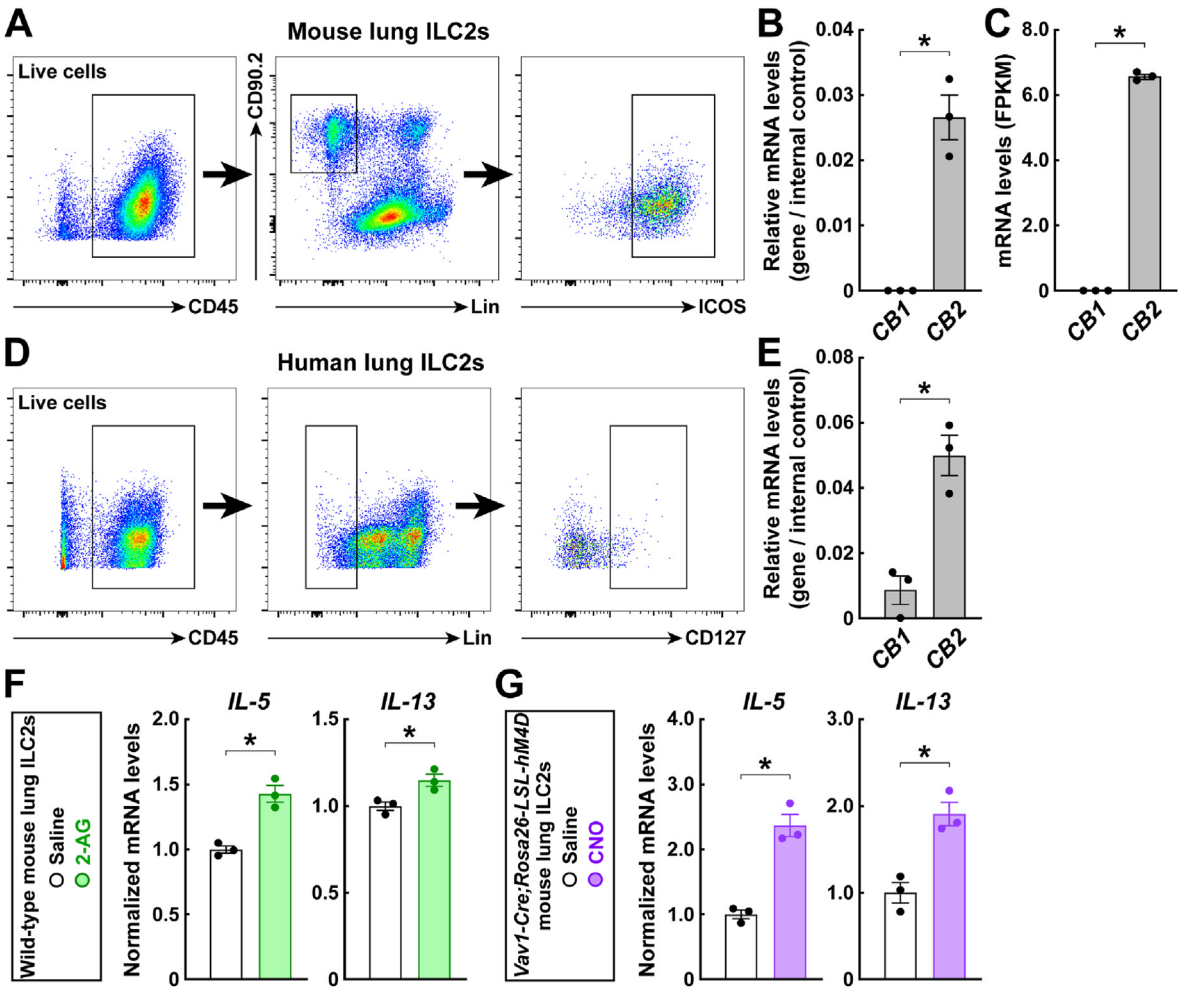

Fig. 1. CB2 and its downstream signal promote the immune response of ILC2s.
(A to C) CB2 is expressed in mouse lung ILC2s. **(A)** FACS sorting of mouse lung ILC2s. **(B)** mRNA levels of *CB1* and *CB2* in mouse lung ILC2s were compared by the qPCR analysis. n = 3, mean ± SEM, *$p < 0.05$ (Student's *t*-test). **(C)** mRNA levels of *CB1* and *CB2* in mouse lung ILC2s were quantified by RNA-Seq. n = 3, mean ± SEM, *$p < 0.05$ (Student's *t*-test). **(D and E)** Human lung ILC2s express CB2. **(D)** FACS sorting of human lung ILC2s. **(E)** mRNA levels of *CB1* and *CB2* in human lung ILC2s were compared by the qPCR analysis. n = 3, mean ± SEM, *$p < 0.05$ (Student's *t*-test). **(F)** The CB2 signal promotes the immune response of ILC2s. ILC2s were FACS-sorted from the lung tissues of wild-type mice and *in vitro* treated with the endocannabinoid 2-arachidonoylglycerol (2-AG) or saline control. mRNA levels of *IL-5* and *IL-13* were assessed by the qPCR analysis and normalized to the saline-treated condition. n = 3, mean ± SEM, *$p < 0.05$ (Student's *t*-test). **(G)** Chemogenetic activation of the Gi signal downstream of CB2 enhances the immune response of ILC2s. ILC2s were FACS-sorted from the lung tissues of *Vav1-Cre; Rosa26-LSL-hM4D* mice and *in vitro* treated with clozapine N-oxide (CNO) or saline control. mRNA levels of *IL-5* and *IL-13* in ILC2s were examined by the qPCR analysis and normalized to the saline-treated condition. n = 3, mean ± SEM, *$p < 0.05$ (Student's *t*-test).

the mRNA levels of *IL-4*, *IL-5*, and *IL-13* in the IL-33-treated condition (Fig. 3D). Also, the protein levels of IL-5 and IL-13 decreased in the IL-33-treated $CB2^{-/-}$ lungs (Fig. 3E). Our recent work has established the advanced imaging technique that enables the 3D visualization of lung inflammation (Liu et al., 2020). This 3D imaging method revealed that the IL-33-elicited recruitment of Siglec-F^{+} immune cells, which were predominantly eosinophils, was significantly reduced in the $CB2^{-/-}$ lungs (Fig. 3F and G). In support of this observation, the FACS analysis showed a decreased amount of eosinophils in the IL-33-treated lungs of $CB2^{-/-}$ compared to $CB2^{+/+}$ mice (Fig. 3H and I). Moreover, the IL-33-elicited lung pathology, particularly inflammation surrounding blood vessels and airways as assessed by hematoxylin and eosin (H&E) staining, was alleviated in the $CB2^{-/-}$ mice (Fig. 3J and K).

CB2 is known to be expressed by multiple types of immune and non-immune cells (Klein et al., 2003). To verify the immunomodulatory role of CB2 in ILC2s, we exploited the procedure of depleting endogenous lung ILC2s (Monticelli et al., 2011). The intraperitoneal administration of the anti-CD90.2 antibody in wild-type C57BL/6 mice carrying the CD90.2 allele could completely ablate ILC2s in the lung tissues (Fig. 4A). The $CB2^{-/-}$ and $CB2^{+/+}$ littermates, which were also on C57BL/6 background carrying CD90.2, were subjected to this anti-CD90.2-mediated ILC2 depletion. Those recipient mice were then adoptively transferred with congenically disparate CD90.1^{+} wild-type lung ILC2s that were resistant to the depleting effect of the anti-CD90.2 antibody. The resulting chimeric mice were intranasally treated with IL-33 to elicit the type 2 immune response. Notably, type 2 cytokines were up-regulated at comparable levels in the lung tissues of chimeric $CB2^{+/+}$ and $CB2^{-/-}$ mice after the IL-33 treatment (Fig. 4B). Also, eosinophil recruitment in the lungs occurred similarly in these two chimeric mice (Fig. 4C), suggesting that the CB2 deletion in immune cells other than ILC2s or in non-immune cells had a minor role in this context. These results demonstrated that the CB2 signal in ILC2s designated the IL-33-elicited immune response in the lung.

We further tested the immunomodulatory role of CB2 in papain-induced lung inflammation, another standard model involving ILC2-mediated innate immunity (Kamijo et al., 2013). Reminiscent to that shown in the IL-33 treatment, the expression levels of *IL-4*, *IL-5*, and *IL-13* markedly decreased in the papain-treated lungs of $CB2^{-/-}$ compared to

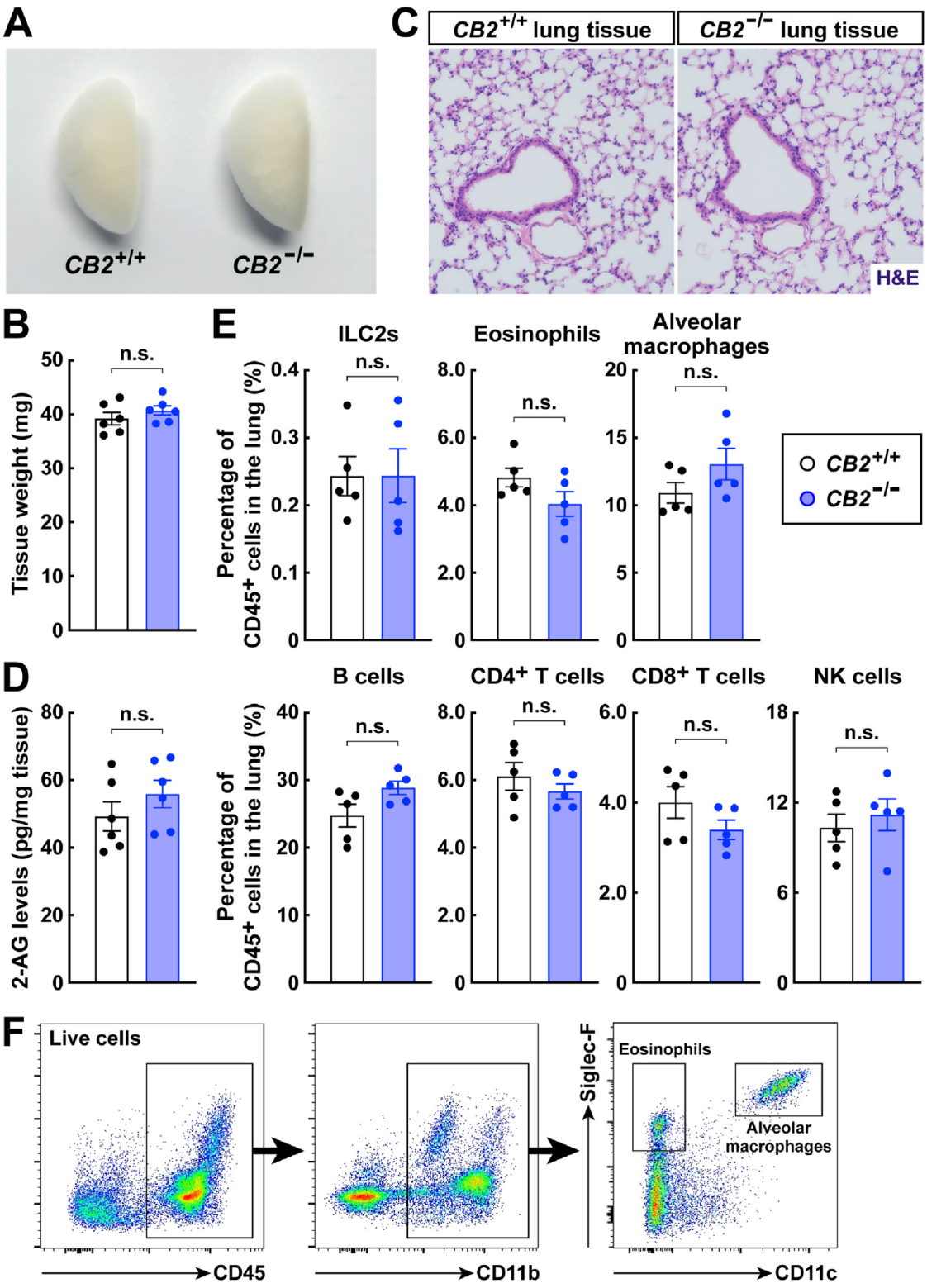

Fig. 2. Genetic deletion of CB2 does not affect the normal development or immune homeostasis of the lung.
(A to C) Normal lung development with the CB2 deletion. **(A)** Gross appearance of the lung tissues (left lobe) of adult $CB2^{-/-}$ and control $CB2^{+/+}$ littermates. **(B)** Tissue weights (left lobe) were measured. n = 6, mean ± SEM, n.s., not significant (Student's *t*-test). **(C)** Representative images of the lung tissue sections of $CB2^{+/+}$ and $CB2^{-/-}$ mice assessed by hematoxylin and eosin (H&E) staining. **(D)** The CB2 deletion does not affect tissue levels of the endocannabinoid 2-AG. 2-AG tissue levels in the lungs of $CB2^{+/+}$ and $CB2^{-/-}$ mice were compared by the ELISA analysis. n = 6, mean ± SEM, n.s., not significant (Student's *t*-test). **(E and F)** Immune cell populations are not affected by the CB2 deletion. **(E)** ILC2s and other immune cell types in the lungs of $CB2^{+/+}$ and $CB2^{-/-}$ mice were examined by the FACS analysis. n = 5, mean ± SEM, n.s., not significant (Student's *t*-test). **(F)** Representative FACS gating of eosinophils ($CD45^+$ $CD11b^+$ $CD11c^-$ Siglec-F^+) and alveolar macrophages ($CD45^+$ $CD11b^+$ $CD11c^+$ Siglec-F^+) in the lung.

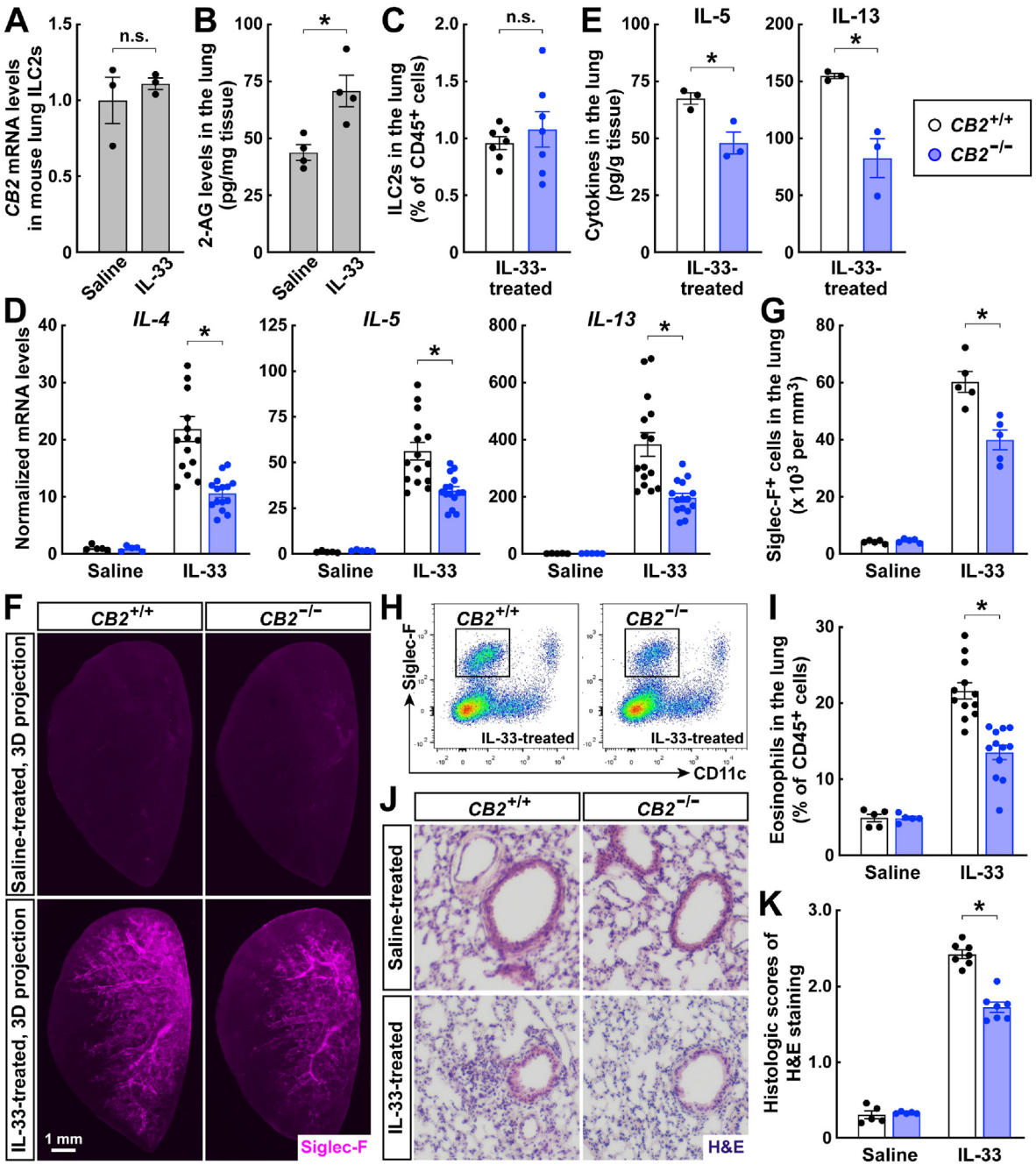

Fig. 3. Genetic deletion of CB2 mitigates the IL-33-elicited type 2 immunity in the lung.

(A and B) Wild-type mice were intranasally treated with IL-33 or control saline. **(A)** ILC2s were FACS-sorted from the saline-treated or IL-33-treated lung tissues, and *CB2* mRNA levels in ILC2s were compared by the qPCR analysis. n = 3, mean ± SEM, n.s., not significant (Student's *t*-test). **(B)** 2-AG levels in the saline-treated or IL-33-treated lung tissues were quantified by the ELISA analysis. n = 4, mean ± SEM, $*p < 0.05$ (Student's *t*-test). **(C to K)** $CB2^{-/-}$ and control $CB2^{+/+}$ littermates were subjected to intranasal IL-33 treatment. **(C)** ILC2s in the IL-33-treated lungs of $CB2^{+/+}$ and $CB2^{-/-}$ mice were examined by the FACS analysis. n = 7, mean ± SEM, n.s., not significant (Student's *t*-test). **(D)** mRNA levels of *IL-4*, *IL-5*, and *IL-13* in the lung tissues of $CB2^{+/+}$ and $CB2^{-/-}$ mice were determined by the qPCR analysis and normalized to the saline-treated $CB2^{+/+}$ condition. n = 5 for saline-treated condition and n = 15 for IL-33-treated condition, mean ± SEM, $*p < 0.05$ (two-way ANOVA test). **(E)** Protein levels of IL-5 and IL-13 in the IL-33-treated lungs of $CB2^{+/+}$ and $CB2^{-/-}$ mice were quantified by the ELISA analysis. n = 3, mean ± SEM, $*p < 0.05$ (Student's *t*-test). **(F and G)** IL-33-elicited immune response in the lung was visualized by advanced 3D imaging. The intact, unsectioned lungs (left lobe) of $CB2^{+/+}$ and $CB2^{-/-}$ mice were processed for the whole-tissue anti-Siglec-F immunolabeling. **(F)** Representative 3D-projection images at 1.26 × magnification of the lightsheet imaging were shown. **(G)** The density of Siglec-F^+ immune cells was quantified. n = 5, mean ± SEM, $*p < 0.05$ (two-way ANOVA test). **(H and I)** Eosinophil recruitment in the lungs of $CB2^{+/+}$ and $CB2^{-/-}$ mice was assessed by the FACS analysis. **(H)** Representative FACS gating of eosinophils ($CD45^+$ $CD11b^+$ $CD11c^-$ Siglec-F^+) in the IL-33-treated condition. **(I)** The percentage of eosinophils in total immune cells was quantified. n = 5 for saline-treated condition and n = 12 for IL-33-treated condition, mean ± SEM, $*p < 0.05$ (two-way ANOVA test). **(J and K)** The lung tissues of $CB2^{+/+}$ and $CB2^{-/-}$ mice were assessed by hematoxylin and eosin (H&E) staining. **(J)** Representative images were shown. **(K)** Histologic scores were determined. n = 5 for saline-treated condition and n = 7 for IL-33-treated condition, mean ± SEM, $*p < 0.05$ (two-way ANOVA test).

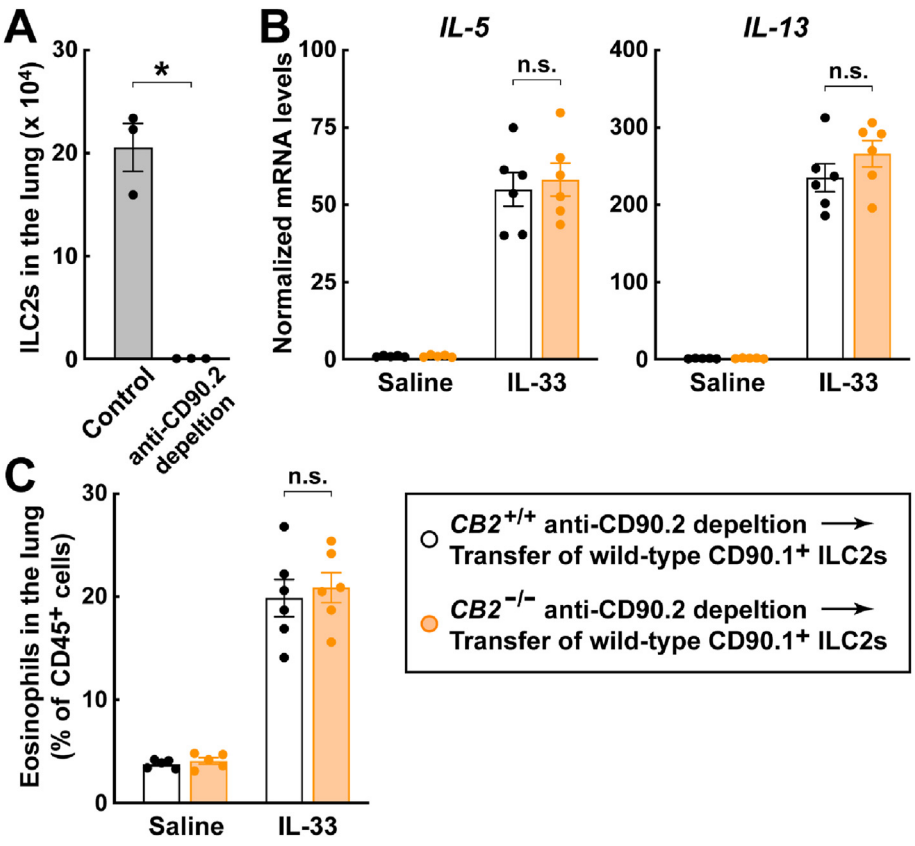

Fig. 4. The CB2 signal in ILC2s designates the IL-33-elicited lung immunity.
(A) Anti-CD90.2-mediated depletion of lung ILC2s. The wild-type C57BL/6 mice carrying CD90.2 were subjected to intranasal IL-33 treatment together with the intraperitoneal administration of the anti-CD90.2 antibody. ILC2s in the lungs were quantified by the FACS analysis. n = 3, mean ± SEM, $*p < 0.05$ (Student's *t*-test). **(B and C)** The CB2 signal in ILC2s designates the IL-33-elicited immune response in the lung. $CB2^{-/-}$ and $CB2^{+/+}$ littermates on C57BL/6 background carrying CD90.2 were intraperitoneally treated with the anti-CD90.2 antibody to deplete endogenous lung ILC2s. Those recipient mice were adoptively transferred with the ILC2s FACS-sorted from wild-type C57BL/6 mice carrying CD90.1 and then subjected to intranasal IL-33 treatment. **(B)** mRNA levels of *IL-5* and *IL-13* in the lung tissues of chimeric mice were determined by the qPCR analysis and normalized to the saline-treated $CB2^{+/+}$-chimeric condition. n = 5 for saline-treated condition and n = 6 for IL-33-treated condition, mean ± SEM, n.s., not significant (two-way ANOVA test). **(C)** Eosinophils in the lungs were assessed by the FACS analysis. n = 5 for saline-treated condition and n = 6 for IL-33-treated condition, mean ± SEM, n.s., not significant (two-way ANOVA test).

$CB2^{+/+}$ mice (Fig. 5A). Also, the whole-tissue 3D imaging showed that the accumulation of Siglec-F^{+} immune cells following the papain treatment was markedly reduced with the CB2 deletion (Fig. 5B and C). This diminished eosinophil recruitment in the papain-treated $CB2^{-/-}$ lungs was confirmed by the FACS analysis (Fig. 5D). In line with such blunted immune responses, the CB2 deletion ameliorated the papain-induced lung pathology as assessed by the histological examination (Fig. 5E and F). These results validated that the CB2 signal would exert a critical role in promoting type 2 immunity during lung damage.

3. Discussion

This study exploited the transcriptomic approach to show that CB2, but not CB1, is highly expressed in mouse and human lung ILC2s. Of importance, pharmacologic or chemogenetic activation of CB2 and its downstream Gi signal could directly promote the IL-33-elicited immune response of lung ILC2s. Conversely, the genetic deletion of CB2 mitigated type 2 innate immunity in response to IL-33, as assessed by the advanced 3D imaging technique in combination with conventional FACS and histologic analyses. These results are in accordance with a recent report that the pharmacologic or genetic blockage of the CB2 signal ameliorated the IL-33-elicited lung pathology (Hurrell et al., 2022). Moreover, we elucidated that the CB2 deletion could similarly reduce the lung inflammation caused by papain exposure, thus demonstrating a critical aspect of the immunomodulation afforded by this cannabinoid receptor.

ILC2s are broadly involved in the immune homeostasis or disease conditions of various organs, e.g., the gastrointestinal tract, liver, and skin (Kim et al., 2016; Meininger et al., 2020). Whether the CB2 signal may modulate ILC2s in those organs remains to be determined. Also, whether CB2 can influence other types of lymphoid cells, e.g., natural killer (NK) cells, ILC1s, and ILC3s, calls for additional investigations. Notably, a prior report showed that the CB2 signal inhibited the IFN-γ production of NK cells, which would otherwise limit the house dust mite-induced lung inflammation in mice (Ferrini et al., 2017). In addition, whether the CB2 signal may participate in antigen-specific adaptive immune responses, e.g., those encountered in allergen-triggered airway hypersensitivity, awaits future studies.

We observed that the genetic deletion of CB2 did not affect the homeostatic levels of 2-AG in mouse lung tissues. However, the IL-33-elicited type 2 immunity led to an increase of 2-AG tissue levels, supporting the pathophysiological relevance of this endocannabinoid in lung immunity. These results have raised several intriguing questions for future research attention. (1) The exact cellular source(s) of 2-AG in the lung has yet to be determined. ILC2s may produce 2-AG by themselves, which then acts in an autocrine manner. Alternatively, other immune cells or non-immune parenchyma cells can supply 2-AG to modulate the immune response of ILC2s. (2) It has been known that the 2-AG metabolism, i.e., its production by diacylglycerol lipase (DAGL) or breakdown by monoacylglycerol lipase (MAGL), is tightly regulated (Baggelaar et al., 2018; Murataeva et al., 2014). Whether this metabolic pathway may become altered by specific disease insults and thereby influence lung inflammation warrants detailed examinations. (3) Studies in the nervous system have documented that the 2-AG production and release are controlled by upstream neural signals. Our recent works with advanced 3D imaging revealed dense neural innervations, including sympathetic and parasympathetic axons, in mouse and primate lungs (Liu et al., 2020). Such local neural inputs may influence the 2-AG availability as a novel neuroimmune mechanism.

Given the immunomodulatory function of CB2, it is a tempting possibility that specific small-molecule antagonists of CB2 represent a novel entry point for treating pulmonary conditions such as asthma. On the other hand, in light of this current study and other works (Hurrell et al., 2022), cannabinoid exposure may aggravate particular lung diseases and become a risk factor for medical or recreational marijuana. Indeed, clinical evidence has begun to implicate that cannabis inhalation could worsen the symptoms of asthma (Chatkin et al., 2019), although more

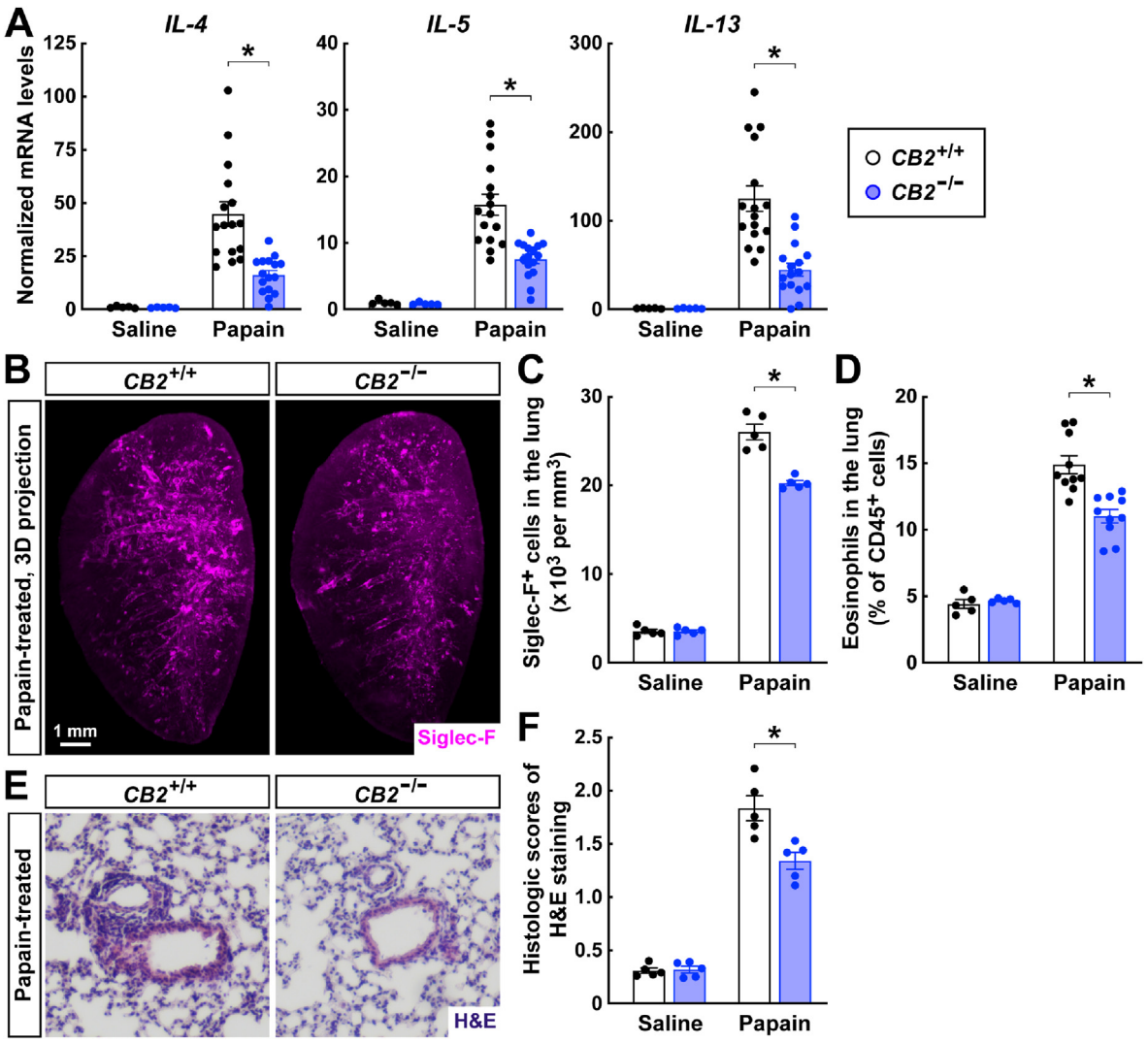

Fig. 5. Blockage of the CB2 signal ameliorates papain-induced lung pathology.
CB2$^{-/-}$ and control *CB2*$^{+/+}$ littermates were subjected to intranasal papain treatment. **(A)** mRNA levels of *IL-4*, *IL-5*, and *IL-13* in the lung tissues of *CB2*$^{+/+}$ and *CB2*$^{-/-}$ mice were determined by the qPCR analysis and normalized to the saline-treated *CB2*$^{+/+}$ condition. n = 5 for saline-treated condition and n = 16 for papain-treated condition, mean ± SEM, *$p < 0.05$ (two-way ANOVA test). **(B and C)** Papain-induced lung inflammation was visualized by advanced 3D imaging. The intact, unsectioned lungs (left lobe) of *CB2*$^{+/+}$ and *CB2*$^{-/-}$ mice were processed for the whole-tissue anti-Siglec-F immunolabeling. **(B)** Representative 3D-projection images at 1.26 × magnification of the lightsheet imaging were shown. **(C)** The density of Siglec-F^{+} immune cells was quantified. n = 5, mean ± SEM, *$p < 0.05$ (two-way ANOVA test). **(D)** Eosinophil recruitment in the lungs of *CB2*$^{+/+}$ and *CB2*$^{-/-}$ mice was examined by the FACS analysis. n = 5 for saline-treated condition and n = 10 for papain-treated condition, mean ± SEM, *$p < 0.05$ (two-way ANOVA test). **(E and F)** The lung tissues of *CB2*$^{+/+}$ and *CB2*$^{-/-}$ mice were assessed by hematoxylin and eosin (H&E) staining. **(E)** Representative images were shown. **(F)** Histologic scores were determined. n = 5, mean ± SEM, *$p < 0.05$ (two-way ANOVA test).

studies are needed to assess its long-term impact on patients.

In sum, we have elucidated the critical role of the CB2 signal in promoting ILC2-mediated type 2 immunity in the lung. These research findings have broad implications for understanding the immunomodulatory effects of the endocannabinoid system as well as cannabis usage.

4. Materials and methods

4.1. Human lung tissues

Human lung tissues were collected in compliance with the protocol approved by the Institutional Ethics Committee of Peking University Third Hospital, and informed consent was signed by each involved patient. The normal lung tissues were obtained during the lobectomy for lung cancer.

Human lung tissues were minced into small pieces on ice and digested in RPMI 1640 medium (Thermo Fisher Scientific) containing 0.1 mg/ml Liberase TL (Roche), 20 μg/ml DNase I (Sigma), 10 mM HEPES, and 3% heat-inactivated fetal bovine serum (HI-FBS; Sigma) at 37 °C for 15 min. The tissues were mashed through a 70-μm cell strainer. The resulting cells were centrifuged at 500 *g* for 5 min and re-suspended in ammonium-chloride-potassium (ACK buffer; Thermo Fisher Scientific) to lyse red blood cells. The cells were centrifuged again at 500 *g* for 5 min and re-suspended in Hanks' balanced salt solution (HBSS; Thermo Fisher Scientific) containing 3% HI-FBS. The cells were then stained by the intended FACS antibodies and sorted on BD FACSAria. Human lung ILC2s were identified as CD45^{+} Lin^{-} CD127^{+} (Lin^{-}: CD3^{-} CD5^{-} CD11b^{-} CD11c^{-} CD14^{-} CD19^{-} FceRI^{-}). Total RNAs of human lung ILC2s were extracted by the RNeasy Mini Kit (Qiagen) and analyzed by the SYBR Green Real-Time PCR Kit (Thermo Fisher Scientific). *Cyclophilin* mRNA levels were utilized as the internal control.

4.2. Mouse information and procedures

All the experimental procedures in mice were performed in compliance with the protocol approved by the Institutional Animal Care and Use Committee (IACUC) of Peking University. Mice were maintained on the 12-h/12-h light/dark cycle (light period 7:00 a.m.–7:00 p.m.), with the standard chow diet and water available *ad libitum*. Mice utilized in experiments were 8- to 12-week-old females. C57BL/6 wild-type mice were purchased from Charles River International. C57BL/6 mice carrying CD90.1 were obtained from the Jackson Laboratory (#000406, RRID:IMSR_JAX:000406) and in-house bred. *Vav1-Cre* (#035670, RRID:IMSR_JAX:035670) and *Rosa26-LSL-hM4D* (#026219, RRID:IMSR_JAX:026219) mouse lines were purchased from the Jackson Laboratory and crossed to produce *Vav1-Cre; Rosa26-LSL-hM4D* mice. *CB2*$^{-/-}$ mouse line was generated with the targeting vector that deleted 426 bp in the coding sequence of exon 2 of the *CB2* gene. The linearized vector was microinjected together with the CRISPR/Cas9 system into fertilized oocytes of C57BL/6 mice. The resulting offspring were screened for the targeted allele and backcrossed with C57BL/6 wild-type mice for two generations to obtain *CB2*$^{+/-}$ mice, which were further bred to produce *CB2*$^{-/-}$ and control *CB2*$^{+/+}$ littermates.

For the IL-33-elicited type 2 immune response in the lung, mice were briefly anesthetized with 3% isoflurane. 2 μg of recombinant mouse IL-33 protein (PeproTech) dissolved in 40 μl of sterile phosphate-buffered saline (PBS) was intranasally administered to each mouse every 24 h twice. The lung tissues were harvested 24 h after the second instillation.

For the papain-induced lung inflammation, mice were briefly anesthetized with 3% isoflurane. 25 μg of papain (Sigma) dissolved in 40 μl of sterile PBS was intranasally administered to each mouse every 24 h for 4 days. The lung tissues were harvested 24 h after the last instillation.

4.3. Whole-tissue immunolabeling and optical clearing

The intact, unsectioned mouse lungs were immunolabeled by the iDISCO(ace) method, as we previously reported (Liu et al., 2020). Briefly, mice were perfused with 20 ml PBS/100 μg/ml heparin followed by 20 ml PBS/1% paraformaldehyde (PFA)/10% sucrose/100 μg/ml heparin. The lungs were dissected out and post-fixed in PBS/1% PFA at room temperature for 2 h. The tissues were washed with PBS at room temperature for 1 h twice and treated at room temperature with 25% acetone (diluted in ddH_2O) for 1 h, 50% acetone for 3 h, and 25% acetone for 1 h. The tissues were washed with PBS at room temperature for 1 h, followed by PBS/30% sucrose for 4 h. The tissues were decolorized in PBS/30% sucrose/1% H_2O_2/10 mM EDTA-Na (pH 8.0) at 4 °C overnight. The tissues were blocked with PBS/0.2% Triton X-100/10% DMSO/5% normal donkey serum at room temperature overnight and then immunolabeled with rat anti-Siglec-F primary antibody (BD Biosciences, Cat#552125, RRID:AB_394340; final concentration of 1 μg/ml) in PBS/0.1% Tween 20/10 μg/ml heparin/5% normal donkey serum at room temperature for 72 h. The tissues were washed with PBS/0.1% Tween 20/10 μg/ml heparin at room temperature for 12 h, with the fresh buffer changed every 2 h. The tissues were further immunolabeled with Alexa Fluor 647-conjugated donkey anti-rat IgG secondary antibody (Thermo Fisher Scientific, Cat#A78947, RRID:AB_2910635; final concentration of 2 μg/ml) in PBS/0.1% Tween 20/10 μg/ml heparin/5% normal donkey serum at room temperature for 72 h. The tissues were washed with PBS/0.1% Tween 20/10 μg/ml heparin at room temperature for 48 h, with the fresh buffer changed every 8 h. All the incubation steps were performed with gentle rotation.

The immunolabeled mouse lungs were embedded in PBS/0.8% agarose for the optical-clearing steps. The tissue blocks were incubated at room temperature with 20% methanol (diluted in ddH_2O) for 1 h three times, 40% methanol for 2 h, 60% methanol for 2 h, 80% methanol for 2 h, 100% methanol for 2 h, and 100% methanol overnight. The tissue blocks were then incubated at room temperature with a mixture of dichloromethane and methanol (v:v = 2:1) for 2 h twice, followed by 100% dichloromethane for 1 h three times. The tissue blocks were finally incubated at room temperature with 100% dibenzyl-ether for 12 h three times. All the incubation steps were performed with gentle rotation.

4.4. Lightsheet 3D imaging

The immunolabeled and optically-cleared mouse lungs were imaged on the LaVision Biotec Ultramicroscope II equipped with the 2 × /NA0.5 objective covered with a 10 mm-working-distance dipping cap. The tissues were immersed in the imaging chamber filled with 100% dibenzyl-ether. Each tissue was scanned at 1.26 × (0.63 × zoom) magnification with a step size of 4 μm by three combined lightsheets from the left side. Imaris (https://imaris.oxinst.com/packages) was used to reconstruct the image stacks obtained from the lightsheet imaging. Three 300 μm × 300 μm × 300 μm cubic volumes were randomly selected along the tertiary bronchi in the reconstructed 3D image of each tissue, and Siglec-F$^+$ immune cells in each cubic volume were manually counted to calculate the cell density. Orthogonal 3D projections were generated for representative images shown in the figures, with a gamma correction of 1.3–1.6 applied to the raw data for display purposes.

4.5. Mouse tissue analyses

For the qPCR analysis, lung tissues were freshly dissected from the mice of indicated conditions. Total RNAs were extracted by the RNeasy Mini Kit and analyzed by the SYBR Green Real-Time PCR Kit. *Cyclophilin* mRNA levels were utilized as the internal control.

For the ELISA analysis of the endocannabinoid 2-arachidonoylglycerol (2-AG), lung tissues were freshly dissected and thoroughly homogenized in PBS on ice. The resulting homogenates were centrifuged at 20,000 *g* for 10 min to clear out tissue debris. 2-AG levels in the supernatants were measured by the Mouse 2-AG Elisa Kit (Krishgen Biosystems).

For the FACS analysis, lung tissues were freshly dissected and minced into small pieces on ice. The tissues were digested in RPMI 1640/0.1 mg/ml Liberase TL/20 μg/ml DNase I/10 mM HEPES/3% HI-FBS at 37 °C for 15 min. The tissues were mashed through a 70-μm cell strainer and centrifuged at 500 *g* for 5 min. The cells were re-suspended in ACK buffer to lyse red blood cells. The cells were centrifuged again at 500 *g* for 5 min and re-suspended in HBSS/3% HI-FBS for staining with the intended FACS antibodies. The immunostained cells were processed on the BD LSRFortessa, and the FACS data were analyzed by FlowJo (https://www.flowjo.com). Immune cell types were identified as follow: eosinophils (CD45$^+$ CD11b$^+$ CD11c$^-$ Siglec-F$^+$), alveolar macrophages (CD45$^+$ CD11b$^+$ CD11c$^+$ Siglec-F$^+$), B cells (CD45$^+$ CD3$^-$ B220$^+$), CD4$^+$ T cells (CD45$^+$ CD3$^+$ CD4$^+$ CD8$^-$ NK1.1$^-$), CD8$^+$ T cells (CD45$^+$ CD3$^+$ CD4$^-$ CD8$^+$ NK1.1$^-$), and NK cells (CD45$^+$ CD3$^-$ NK1.1$^+$).

For the histological analysis, lung tissues were harvested and post-fixed in PBS/4% PFA at room temperature overnight. The tissues were processed for paraffin sectioning and hematoxylin and eosin (H&E) staining. Histologic scores were then determined according to the published criteria (Kelly-Welch et al., 2004) with minor modifications. Ten examined areas (20 × magnification) were randomly selected from the H&E sections of each tissue: 0, no sign of cellular infiltration; 1, light and dispersed infiltration surrounding <10% of blood vessels and airways; 2, moderate infiltration surrounding 10%–50% of blood vessels and airways; 3, heavy and focused infiltration surrounding >50% of blood vessels and airways.

4.6. Mouse ILC2s

Mouse lung tissues were processed for the FACS staining as above and sorted on BD FACSAria. Mouse lung ILC2s were identified as CD45$^+$ Lin$^-$ CD90.2$^+$ ICOS$^+$ (Lin$^-$: CD3$^-$ CD4$^-$ CD8a$^-$ CD11b$^-$ CD11c$^-$ CD19$^-$ Gr-1$^-$ NK1.1$^-$ TCRβ$^-$ TCRγδ$^-$ TER119$^-$). Total RNAs of mouse lung ILC2s were extracted by the RNeasy Mini Kit and analyzed by the SYBR Green Real-

Time PCR Kit with *Cyclophilin* mRNA levels as the internal control. In parallel, mouse lung ILC2s were subjected to single-end RNA-Seq analyses by the Beijing Genomics Institute. Gene expression levels were normalized as fragments per kilobase per million (FPKM). The RNA-Seq data were deposited to the BioSample Database (https://www.ncbi.nlm.nih.gov/sra) with the accession numbers SRX21368054, SRX21368055, and SRX21368056.

For the ILC2 adoptive transfer, recipient *CB2*$^{-/-}$ and control *CB2*$^{+/+}$ littermates (on C57BL/6 background carrying CD90.2) were intraperitoneally injected with the anti-CD90.2 antibody (Bio X Cell) at 10 mg/kg of body weight every 24 h twice to deplete endogenous lung ILC2s. Donor ILC2s [CD45^{+} Lin^{-} CD90.1^{+} ICOS^{+} (Lin^{-}: CD3^{-} CD4^{-} CD8a^{-} CD11b^{-} CD11c^{-} CD19^{-} Gr-1^{-} NK1.1^{-} TCRβ^{-} TCRγδ^{-} TER119^{-})] were obtained from the lung tissues of wild-type C57BL/6 mice carrying CD90.1. Each anti-CD90.2-treated *CB2*$^{-/-}$ or *CB2*$^{+/+}$ mouse was intravenously transferred with 5×10^5 CD90.1^{+} lung ILC2s and simultaneously administered with 20 μg of recombinant mouse IL-33 protein via intraperitoneal injection. 24 h after the ILC2 adoptive transfer, the chimeric mice were subjected to intranasal IL-33 treatment as above.

For the *in vitro* manipulation of the CB2 signal, ILC2s were FACS-sorted from the lungs of indicated mice following intranasal IL-33 treatment as above. Mouse lung ILC2s were rested in RPMI 1640 medium containing 2 mM L-glutamine, 1% insulin-transferrin-selenium (Thermo Fisher Scientific), 100 U/ml penicillin, 100 μg/ml streptomycin, and 2 μM forskolin (Sigma) at 37 °C for 2 h. The cells were then treated with a final concentration of 20 μM 2-AG (Cayman) or 20 μM clozapine N-oxide (CNO; Sigma) for 2 h. Total RNAs of mouse lung ILC2s were extracted by the RNeasy Mini Kit and analyzed by the SYBR Green Real-Time PCR Kit with *Cyclophilin* mRNA levels as the internal control.

4.7. Statistical methods

Student's *t*-test (two-tailed) or ANOVA test (two-way with *post hoc* tests) was performed using GraphPad Prism 8.4.3 (http://www.graphpad.com/scientific-software/prism). All the data points represent biological replicates. Statistical details of the experiments are included in figure legends.

Author statement

J.Y. conceived and designed this study as the corresponding author. T.L., J.L., H.C., and Y.C. performed the experiments and analyzed the results under J.Y.'s supervision. X.Z. and W.F. provided the human tissues.

Declaration of competing interest

The authors declare that they have no known competing financial interests or personal relationships that could have appeared to influence the work reported in this paper.

Acknowledgments

This work has been supported by the National Natural Science Foundation of China (#32100924 to T.L.; #32125017 and #32150008 to J.Y.), the Beijing Natural Science Foundation (#7232086 to J.Y; #7234378 to Y.C.), and the China Postdoctoral Science Foundation (#2022M710219 to Y.C.). T.L. and Y.C. have also been supported by the Postdoctoral Fellowship of the Center for Life Sciences at Peking University. Additional funds to J.Y. have been from the Center for Life Sciences at Peking University, the State Key Laboratory of Membrane Biology at Peking University, and the Institute of Molecular Physiology at Shenzhen Bay Laboratory. The authors declare no conflict of interest.

References

Akdis, C. A., Arkwright, P. D., Bruggen, M. C., Busse, W., Gadina, M., Guttman-Yassky, E., Kabashima, K., Mitamura, Y., Vian, L., Wu, J., & Palomares, O. (2020). Type 2 immunity in the skin and lungs. *Allergy, 75*, 1582–1605. https://doi.org/10.1111/all.14318

Artis, D., & Spits, H. (2015). The biology of innate lymphoid cells. *Nature, 517*, 293–301. https://doi.org/10.1038/nature14189

Baggelaar, M. P., Maccarrone, M., & van der Stelt, M. (2018). 2-Arachidonoylglycerol: A signaling lipid with manifold actions in the brain. *Progress in Lipid Research, 71*, 1–17. https://doi.org/10.1016/j.plipres.2018.05.002

Barlow, J. L., & McKenzie, A. N. J. (2019). Innate lymphoid cells of the lung. *Annual Review of Physiology, 81*, 429–452. https://doi.org/10.1146/annurev-physiol-020518-114630

Barnes, P. J. (2008). Immunology of asthma and chronic obstructive pulmonary disease. *Nature Reviews Immunology, 8*, 183–192. https://doi.org/10.1038/nri2254

Chatkin, J. M., Zani-Silva, L., Ferreira, I., & Zamel, N. (2019). Cannabis-associated asthma and allergies. *Clinical Reviews in Allergy and Immunology, 56*, 196–206. https://doi.org/10.1007/s12016-017-8644-1

Chu, C., Parkhurst, C. N., Zhang, W., Zhou, L., Yano, H., Arifuzzaman, M., & Artis, D. (2021). The ChAT-acetylcholine pathway promotes group 2 innate lymphoid cell responses and anti-helminth immunity. *Science Immunology, 6*. https://doi.org/10.1126/sciimmunol.abe3218

Di Marzo, V. (2008). Targeting the endocannabinoid system: To enhance or reduce? *Nature Reviews Drug Discovery, 7*, 438–455. https://doi.org/10.1038/nrd2553

Di Marzo, V., Bifulco, M., & De Petrocellis, L. (2004). The endocannabinoid system and its therapeutic exploitation. *Nature Reviews Drug Discovery, 3*, 771–784. https://doi.org/10.1038/nrd1495

Do, Y., McKallip, R. J., Nagarkatti, M., & Nagarkatti, P. S. (2004). Activation through cannabinoid receptors 1 and 2 on dendritic cells triggers NF-kappaB-dependent apoptosis: Novel role for endogenous and exogenous cannabinoids in immunoregulation. *Journal of Immunology, 173*, 2373–2382. https://doi.org/10.4049/jimmunol.173.4.2373

Eberl, G., Colonna, M., Di Santo, J. P., & McKenzie, A. N. (2015). Innate lymphoid cells. Innate lymphoid cells: A new paradigm in immunology. *Science, 348*, aaa6566. https://doi.org/10.1126/science.aaa6566

Ferrini, M. E., Hong, S., Stierle, A., Stierle, D., Stella, N., Roberts, K., & Jaffar, Z. (2017). CB2 receptors regulate natural killer cells that limit allergic airway inflammation in a murine model of asthma. *Allergy, 72*, 937–947. https://doi.org/10.1111/all.13107

Gieseck, R. L., 3rd, Wilson, M. S., & Wynn, T. A. (2018). Type 2 immunity in tissue repair and fibrosis. *Nature Reviews Immunology, 18*, 62–76. https://doi.org/10.1038/nri.2017.90

Hammad, H., & Lambrecht, B. N. (2015). Barrier epithelial cells and the control of type 2 immunity. *Immunity, 43*, 29–40. https://doi.org/10.1016/j.immuni.2015.07.007

Holt, P. G., Strickland, D. H., Wikstrom, M. E., & Jahnsen, F. L. (2008). Regulation of immunological homeostasis in the respiratory tract. *Nature Reviews Immunology, 8*, 142–152. https://doi.org/10.1038/nri2236

Hurrell, B. P., Helou, D. G., Shafiei-Jahani, P., Howard, E., Painter, J. D., Quach, C., & Akbari, O. (2022). Cannabinoid receptor 2 engagement promotes group 2 innate lymphoid cell expansion and enhances airway hyperreactivity. *The Journal of Allergy and Clinical Immunology, 149*, 1628–1642. https://doi.org/10.1016/j.jaci.2021.09.037. e1610.

Iwasaki, A., Foxman, E. F., & Molony, R. D. (2017). Early local immune defences in the respiratory tract. *Nature Reviews Immunology, 17*, 7–20. https://doi.org/10.1038/nri.2016.117

Kamijo, S., Takeda, H., Tokura, T., Suzuki, M., Inui, K., Hara, M., Matsuda, H., Matsuda, A., Oboki, K., Ohno, T., et al. (2013). IL-33-mediated innate response and adaptive immune cells contribute to maximum responses of protease allergen-induced allergic airway inflammation. *Journal of Immunology, 190*, 4489–4499. https://doi.org/10.4049/jimmunol.1201212

Kelly-Welch, A. E., Melo, M. E., Smith, E., Ford, A. Q., Haudenschild, C., Noben-Trauth, N., & Keegan, A. D. (2004). Complex role of the IL-4 receptor alpha in a murine model of airway inflammation: Expression of the IL-4 receptor alpha on nonlymphoid cells of bone marrow origin contributes to severity of inflammation. *Journal of Immunology, 172*, 4545–4555. https://doi.org/10.4049/jimmunol.172.7.4545

Kim, C. H., Hashimoto-Hill, S., & Kim, M. (2016). Migration and tissue tropism of innate lymphoid cells. *Trends in Immunology, 37*, 68–79. https://doi.org/10.1016/j.it.2015.11.003

Klein, T. W., Newton, C., Larsen, K., Lu, L., Perkins, I., Nong, L., & Friedman, H. (2003). The cannabinoid system and immune modulation. *Journal of Leukocyte Biology, 74*, 486–496. https://doi.org/10.1189/jlb.0303101

Klein, T. W., Newton, C. A., Nakachi, N., & Friedman, H. (2000). Delta 9-tetrahydrocannabinol treatment suppresses immunity and early IFN-gamma, IL-12, and IL-12 receptor beta 2 responses to Legionella pneumophila infection. *Journal of Immunology, 164*, 6461–6466. https://doi.org/10.4049/jimmunol.164.12.6461

Klose, C. S. N., Mahlakoiv, T., Moeller, J. B., Rankin, L. C., Flamar, A. L., Kabata, H., Monticelli, L. A., Moriyama, S., Putzel, G. G., Rakhilin, N., et al. (2017). The neuropeptide neuromedin U stimulates innate lymphoid cells and type 2 inflammation. *Nature, 549*, 282–286. https://doi.org/10.1038/nature23676

Kondo, Y., Yoshimoto, T., Yasuda, K., Futatsugi-Yumikura, S., Morimoto, M., Hayashi, N., Hoshino, T., Fujimoto, J., & Nakanishi, K. (2008). Administration of IL-33 induces airway hyperresponsiveness and goblet cell hyperplasia in the lungs in the absence of adaptive immune system. *International Immunology, 20*, 791–800. https://doi.org/10.1093/intimm/dxn037

Liu, T., Yang, L., Han, X., Ding, X., Li, J., & Yang, J. (2020). Local sympathetic innervations modulate the lung innate immune responses. *Science Advances, 6*, Article eaay1497. https://doi.org/10.1126/sciadv.aay1497

Lloyd, C. M., & Marsland, B. J. (2017). Lung homeostasis: Influence of age, microbes, and the immune system. *Immunity, 46*, 549–561. https://doi.org/10.1016/j.immuni.2017.04.005

Lu, H. C., & Mackie, K. (2021). Review of the endocannabinoid system. *Biological Psychiatry: Cognitive Neuroscience and Neuroimaging, 6*, 607–615. https://doi.org/10.1016/j.bpsc.2020.07.016

Mackie, K. (2008). Cannabinoid receptors: Where they are and what they do. *Journal of Neuroendocrinology, 20*(Suppl 1), 10–14. https://doi.org/10.1111/j.1365-2826.2008.01671.x

Mechoulam, R., & Parker, L. A. (2013). The endocannabinoid system and the brain. *Annual Review of Psychology, 64*, 21–47. https://doi.org/10.1146/annurev-psych-113011-143739

Meininger, I., Carrasco, A., Rao, A., Soini, T., Kokkinou, E., & Mjosberg, J. (2020). Tissue-specific features of innate lymphoid cells. *Trends in Immunology, 41*, 902–917. https://doi.org/10.1016/j.it.2020.08.009

Monticelli, L. A., Sonnenberg, G. F., Abt, M. C., Alenghat, T., Ziegler, C. G., Doering, T. A., Angelosanto, J. M., Laidlaw, B. J., Yang, C. Y., Sathaliyawala, T., et al. (2011). Innate lymphoid cells promote lung-tissue homeostasis after infection with influenza virus. *Nature Immunology, 12*, 1045–1054. https://doi.org/10.1031/ni.2131

Moriyama, S., Brestoff, J. R., Flamar, A. L., Moeller, J. B., Klose, C. S. N., Rankin, L. C., Yudanin, N. A., Monticelli, L. A., Putzel, G. G., Rodewald, H. R., & Artis, D. (2018). beta2-adrenergic receptor-mediated negative regulation of group 2 innate lymphoid cell responses. *Science, 359*, 1056–1061. https://doi.org/10.1126/science.aan4829

Murataeva, N., Straiker, A., & Mackie, K. (2014). Parsing the players: 2-arachidonoylglycerol synthesis and degradation in the CNS. *British Journal of Pharmacology, 171*, 1379–1391. https://doi.org/10.1111/bph.12411

Pacula, R. L., & Smart, R. (2017). Medical marijuana and marijuana legalization. *Annual Review of Clinical Psychology, 13*, 397–419. https://doi.org/10.1146/annurev-clinpsy-032816-045128

Page, R. L., 2nd, Allen, L. A., Kloner, R. A., Carriker, C. R., Martel, C., Morris, A. A., Piano, M. R., Rana, J. S., Saucedo, J. F., et al., American Heart Association Clinical Pharmacology, C. (2020). Medical marijuana, recreational cannabis, and cardiovascular health: A scientific statement from the American heart association. *Circulation, 142*, e131–e152. https://doi.org/10.1161/CIR.0000000000000883

Rodriguez-Rodriguez, N., Gogoi, M., & McKenzie, A. N. J. (2021). Group 2 innate lymphoid cells: Team players in regulating asthma. *Annual Review of Immunology, 39*, 167–198. https://doi.org/10.1146/annurev-immunol-110119-091711

Shivers, S. C., Newton, C., Friedman, H., & Klein, T. W. (1994). Delta 9-Tetrahydrocannabinol (THC) modulates IL-1 bioactivity in human monocyte/macrophage cell lines. *Life Sciences, 54*, 1281–1289. https://doi.org/10.1016/0024-3205(94)00856-6

Sui, P., Wiesner, D. L., Xu, J., Zhang, Y., Lee, J., Van Dyken, S., Lashua, A., Yu, C., Klein, B. S., Locksley, R. M., et al. (2018). Pulmonary neuroendocrine cells amplify allergic asthma responses. *Science, 360*. https://doi.org/10.1126/science.aan8546

Tanasescu, R., & Constantinescu, C. S. (2010). Cannabinoids and the immune system: An overview. *Immunobiology, 215*, 588–597. https://doi.org/10.1016/j.imbio.2009.12.005

Wallrapp, A., Riesenfeld, S. J., Burkett, P. R., Abdulnour, R. E., Nyman, J., Dionne, D., Hofree, M., Cuoco, M. S., Rodman, C., Farouq, D., et al. (2017). The neuropeptide NMU amplifies ILC2-driven allergic lung inflammation. *Nature, 549*, 351–356. https://doi.org/10.1038/nature24029